Nonlinear Dyn (2009) 55: 67–78
DOI 10.1007/s11071-008-9345-3

ORIGINAL PAPER

Amplitude reduction of primary resonance of nonlinear oscillator by a dynamic vibration absorber using nonlinear coupling

Hoonhee Jo · Hiroshi Yabuno

Received: 23 May 2007 / Accepted: 21 February 2008 / Published online: 6 March 2008

Abstract The paper presents the characteristics of a new type of nonlinear dynamic vibration absorber for a main system subjected to a nonlinear restoring force under primary resonance. The absorber is connected to the main system by a link in order to be excited with twice the frequency of the motion of the main system. The natural frequency of the absorber is tuned to be twice the natural frequency of the main system, in contrast to autoparametric vibration absorber, whose natural frequency is tuned to be one-half the natural frequency of the main system. The presented absorber is not excited through the autoparametric resonance, i.e., no trivial equilibrium state exists. Therefore, the absorber always oscillates because of the motion of the main system and cannot be trapped by Coulomb friction acting on the absorber, in contrast to the autoparametric vibration absorber. Under small excitation amplitude, this absorber does not produce an overhang in the frequency response curve, which occurs because of the use of the conventional autoparametric vibration absorber; the overhang renders the response amplitude larger than that in the case without an absorber. In addition, the absorber removes the hysteresis in the frequency response curve caused by the nonlinearity of the restoring force acting on the main system. Regarding large excitation amplitude, the response amplitude in the main system can be decreased by increasing the damping of the absorber, but that decrease is limited by the nonlinearity in the restoring force acting on the main system. This paper also describes experimental validation of the absorber under small excitation amplitude using a simple apparatus.

Keywords Nonlinear vibration absorber · Nonlinear coupling · Internal resonance · Primary resonance

H. Jo (✉) · H. Yabuno
Graduate School of Systems and Information Engineering, University of Tsukuba, Tsukuba, 305-8573, Japan
e-mail: johoonhee@aosuna.esys.tsukuba.ac.jp

1 Introduction

Nonlinear vibration absorbers have received much attention along with the advance of nonlinear analytical methods. Haxton and Barr [1] first introduced and studied so-called autoparametric vibration absorber using 2:1 internal resonance between the main system and the absorber [2]. The natural frequency of the absorber is tuned to be about one-half the natural frequency of the main system. In the case of a conventional pendulum-type vibration absorber, the motions of the main system and the absorber correspond, respectively, to the first and second modes. Then autoparametric resonance in the absorber is produced by the motion of the main system. The energy transfer of the main system into the absorber reduces the response amplitude of the resonant main system.

Vyas and Bajaj [3] and Vyas et al. [4, 5] theoretically and experimentally investigated the effectiveness of an autoparametric vibration absorber in a wide frequency range using multiple pendulums. Mustafa and Ertas [6] showed theoretically the effect of the pendulum as an autoparametric vibration absorber in the case where the main system is in parametric resonance. Cuvalci and Ertas [7] investigated both theoretically and experimentally the dynamic behavior of a beam-tip mass-pendulum system with various pendulum damping coefficients and beam-pendulum mass ratios for primary resonance. Mook et al. [8] reported that an autoparametric vibration absorber stabilizes 1/2-order subharmonic resonance for a general multiple-degrees-of-freedom system. Yabuno et al. [9] described both theoretically and experimentally an autoparametric vibration absorber that stabilizes 1/3-order subharmonic resonance against any disturbance. Nayfeh and Mook [10] and Nayfeh [11] compiled a comprehensive survey of internal resonance and autoparametric vibration absorber. The autoparametric vibration absorber produces an overhang in the frequency response, which is independent of the amount of the external excitation amplitude. It makes the response amplitude larger than that in the case without an absorber in an excitation frequency range. Furthermore, the autoparametric vibration absorber has a trivial steady state. In the case where the absorber is not moved because of unexpected effects, as well as Coulomb friction acting on the absorber (e.g., inherently existing Coulomb friction at the supporting point in the case of a pendulum-type autoparametric vibration absorber), the absorber cannot reduce the response amplitude of the main system.

We utilize a different aspect of the internal resonance to overcome that drawback in the autoparametric vibration absorber. We consider an absorber which oscillates because of the quadratic nonlinear coupling with the main system, but that oscillation is not attributable to the autoparametric resonance. The motions of the main system and the absorber correspond to the first and second modes, respectively. In addition, the natural frequency of the absorber is tuned to be twice the natural frequency of the main system [12]. A different configuration of the absorber from autoparametric vibration absorber is necessary to realize such an absorber.

In this paper, we propose a new type of vibration absorber that is connected to the main system by a link. We theoretically analyze the efficiency of the absorber to the primary resonance of the main system, subjected to the cubic nonlinear restoring force. For a small excitation amplitude, the absorber does not produce an overhang in the frequency response curve; for the case of large excitation amplitude, the increased damping of the absorber limits the response amplitude to a small value. Furthermore, results clarify that the nonlinearity of the restoring force acting to the main system decreases the efficiency of the absorber when the excitation amplitude is large. For the case in which the main system is supported by a linear restoring force, the absorber can reduce the response amplitude independently of the magnitude of the excitation amplitude. Finally, the efficiency of the absorber is examined experimentally using a simple apparatus.

2 Analytical model and equations of motion

2.1 Configuration of proposed vibration absorber

We introduce a main system subjected to a nonlinear restoring force (Fig. 1). We set the origin O of a static Cartesian coordinate x–y–z at a point p on the main system in the static equilibrium state. The mass M can be moved freely only in the y-direction. The motion of the main system is expressed by the displacement y of point p from the origin O in the y-direction. We move magnet A as $y_o = a_e \cos Nt$ in the y-direction. The repulsive forces act between magnet B' on the main system and fixed magnet A', and between magnet B on the main system and moved magnet A.

We propose the following absorber, which oscillates with twice the frequency of the motion of the main system. A mass m_o is connected to the point p on the main system through a link; it can be moved freely only in the x-direction. A pendulum with tip mass m is attached to the mass m_o as a nonlinear dynamic vibration absorber. The motion is expressed in terms of the angle θ about point q on the z–x plane.

2.2 Magnetical nonlinear restoring force

Using Fig. 2, we calculate the repulsive force acting between the sinusoidally moved magnet A and magnet B on the main system. The repulsive force in the η-direction between the total magnetic poles on the surface S_2 of magnet A and the total magnetic poles

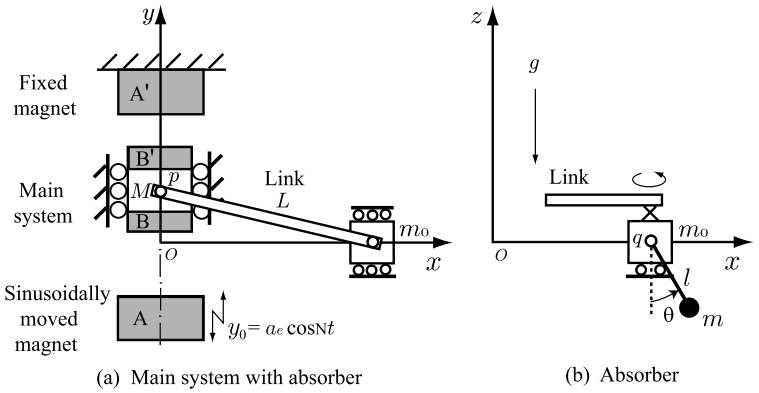

(a) Main system with absorber (b) Absorber

Fig. 1 Analytical model of a nonlinear dynamic vibration absorber

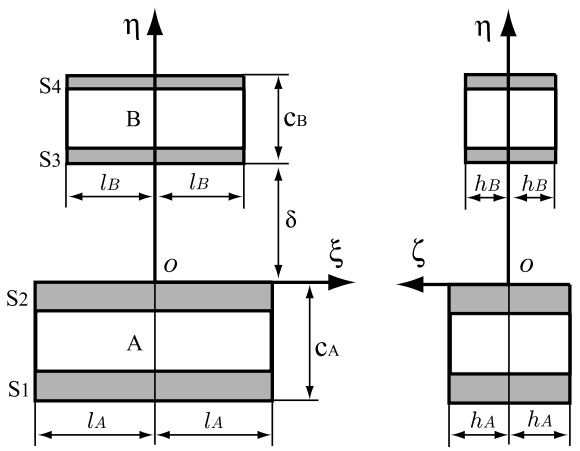

Fig. 2 Repelling magnets on the main system

on the surface S_3 of magnet B is obtained as (1) by integrating Coulomb's law under the following assumption. $\xi_B, |h_A - \eta_B|, |h_A + \eta_B| \ll |\zeta_B - l_A|, |\zeta_B + l_A|$. Therein, (ξ_B, η_B, ζ_B) is a point of surface S_3 [13, 14], and

$$
\begin{aligned}
F(\delta) = \frac{\lambda_A \lambda_B l_B}{2\pi\mu}\Bigg[& 2h_A \tan^{-1}\left(\frac{h_A + h_B}{\delta}\right) \\
& + 2h_B \tan^{-1}\left(\frac{h_A + h_B}{\delta}\right) \\
& - 2h_A \tan^{-1}\left(\frac{h_A - h_B}{\delta}\right) \\
& + 2h_B \tan^{-1}\left(\frac{h_A - h_B}{\delta}\right) \\
& - \delta \log\left\{1 + \left(\frac{h_A + h_B}{\delta}\right)^2\right\} \\
& + \delta \log\left\{1 + \left(\frac{h_A - h_B}{\delta}\right)^2\right\}\Bigg],
\end{aligned} \tag{1}
$$

where δ denotes the gap between magnets A and B. In addition, λ_A, λ_B and μ respectively signify the magnetic flux density of magnets A and B, and magnetic permeability. The repulsive force acting between surface S_1 and S_4 and the absorptive forces acting between surfaces S_1 and S_3, and S_2 and S_4 must also be calculated. Taking into account the thickness c_A and c_B of the magnets, we calculate four forces for the four sets of surfaces using (1). Summing the four forces where the repulsive forces are regarded as positive and where the absorptive ones are regarded as negative yields the repulsive force acting on magnets A and B with gap δ. Using the result given above, we derive a nonlinear restoring force acting on the main system. Here we do not consider the forces between magnets A and A', A and B', A' and B, B and B'. In Fig. 3, we set another static Cartesian coordinate system whose O' is at the upper area of the sinusoidally moved magnet A in the initial static equilibrium state. Here, l is the constant gap between magnets A and A' in the initial static equilibrium state. In addition, l_0 denotes the width of a mass M including magnets B and B'. We consider the motion of the main system around Y_{st}, which is the gap between magnets A and B, i.e., around the initial static equilibrium state. The forces acting on magnets B and B', i.e., $F_B(Y) := F(Y - y_0)$ and $F_{B'}(Y) := F(l - l_0 - Y)$, are expanded with respect to y/Y_{st}, where $Y = Y_{st} + y$ and $|y/Y_{st}| \ll 1$ are assumed. By considering up to the third power of y/Y_{st} and $(y - y_0)/Y_{st}$, we obtain the following equa-

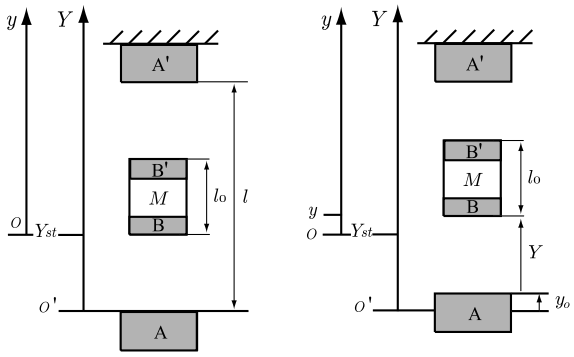

(a) Equilibrium state (b) Sinusoidally excited state

Fig. 3 Analytical model of a nonlinear spring—mass system

tion of motion:

$$\begin{aligned} M\frac{d^2y}{dt^2} &= F_B(Y) - F'_B(l-l_0-Y) \\ &= F(Y_{st}+y-y_0) - F(l-l_0-Y_{st}-y) \\ &= -(K_{R1}+K_{L1})y - (K_{R2}-K_{L2})y^2 \\ &\quad -(K_{R3}+K_{L3})y^3 + K_{R1}y_0 \\ &\quad +2K_{R2}y_0y - K_{R2}{y_0}^2 + 3K_{R3}y_0y^2 \\ &\quad -3K_{R3}{y_0}^2y + K_{R3}{y_0}^3, \end{aligned} \tag{2}$$

where

$$\begin{aligned} K_{R1} &= -\frac{dF_B}{dY}\bigg|_{Y=Y_{st}}, \quad K_{R2} = -\frac{1}{2}\frac{d^2F_B}{dY^2}\bigg|_{Y=Y_{st}}, \\ K_{R3} &= -\frac{1}{6}\frac{d^3F_B}{dY^3}\bigg|_{Y=Y_{st}}, \\ K_{L1} &= -\frac{dF_{B'}}{dY}\bigg|_{Y=Y_{st}}, \quad K_{L2} = -\frac{1}{2}\frac{d^2F_{B'}}{dY^2}\bigg|_{Y=Y_{st}}, \\ K_{L3} &= -\frac{1}{6}\frac{d^3F_{B'}}{dY^3}\bigg|_{Y=Y_{st}}. \end{aligned} \tag{3}$$

2.3 Equations of motion

Equations of motion of the main system subjected to the nonlinear restoring force and of the absorber in Fig. 1 are obtained using a Lagrange's equation. The kinetic and potential energy of the combined system are expressed as

$$\begin{aligned} T &= \frac{1}{2}M\left(\frac{dy}{dt}\right)^2 + \frac{1}{2}m_0\left\{\left(\frac{d}{dt}\frac{y^2}{2L}\right)^2 + \left(\frac{d}{dt}y_0\right)^2\right\} \\ &\quad + \frac{1}{2}m\left\{\frac{d}{dt}\left(\frac{y^2}{2L} + l\sin\theta\right)\right\}^2 \\ &\quad + \frac{1}{2}m\left\{\frac{d}{dt}(y_0 - l\cos\theta)\right\}^2, \end{aligned} \tag{4}$$

$$\begin{aligned} V &= \frac{1}{2}K_{R1}(y-y_0)^2 + \frac{1}{3}K_{R2}(y-y_0)^3 \\ &\quad + \frac{1}{4}K_{R3}(y-y_0)^4 + \frac{1}{2}K_{L1}y^2 + \frac{1}{3}K_{L2}y^3 \\ &\quad + \frac{1}{4}K_{L3}y^4 + mgl(1-\cos\theta), \end{aligned} \tag{5}$$

where the approximation of $L-\sqrt{L^2-y^2} \approx y^2/2L$ is used. From these equations, we have the equations of motion of the main system and the absorber as follows.

$$\begin{aligned} &M\ddot{y} + (K_{R1}+K_{L1})y + (K_{R2}-K_{L2})y^2 \\ &\quad + (K_{R3}+K_{L3})y^3 \\ &= -\frac{m_0+m}{L^2}\left(y\dot{y}^2 - y^2\ddot{y}\right) \\ &\quad - \frac{ml}{L}\left(y\cos\theta\ddot{\theta} + y\sin\theta\dot{\theta}^2\right) \\ &\quad + K_{R1}y_0 + 2K_{R2}y_0y - K_{R2}{y_0}^2 + 3K_{R3}y_0y^2 \\ &\quad - 3K_{R3}{y_0}^2y + K_{R3}{y_0}^3, \end{aligned} \tag{6}$$

$$\begin{aligned} &ml^2\ddot{\theta} + mgl\sin\theta \\ &= -ml(\ddot{y_0}\sin\theta - \dot{y_0}\dot{\theta}\cos\theta) - \frac{ml}{L}y\dot{y}\dot{\theta}^2\sin\theta \\ &\quad + ml\dot{y_0}\dot{\theta}^2\cos\theta \\ &\quad - \frac{ml}{L}\left(\dot{y}^2\cos\theta + y\ddot{y}\cos\theta + y\dot{y}\dot{\theta}\sin\theta\right). \end{aligned} \tag{7}$$

We expand $\sin\theta$ and $\cos\theta$ up to the third power with respect to θ. Equations (6) and (7) are normalized as (8) and (9) by Y_{st} and $1/\sqrt{(K_{R1}+K_{L1})/M}$ ($y/Y_{st} \equiv y^*$ and $t/T \equiv t^*$).

$$\begin{aligned} &\ddot{y^*} + 2\mu_1\dot{y^*} + y^* \\ &= -C_1\ddot{\theta}y^* + C_2\left(y^*\dot{y^*}^2 + {y^*}^2\ddot{y^*}\right) - \alpha_2{y^*}^2 \\ &\quad - 2k_{R2}a_e^*\cos\nu t y^* \\ &\quad - \alpha_3{y^*}^3 - k_{R2}{a_e^*}^2\cos^2\nu t^* + k_{R3}a_e^*\cos\nu t^*{y^*}^2 \\ &\quad - k_{R3}{a_e^*}^2\cos^2\nu t^* y^* \\ &\quad + k_{R3}{a_e^*}^3\cos^3\nu t^* + k_{R1}a_e^*\cos\nu t^*, \end{aligned} \tag{8}$$

$$\ddot{\theta} + 2\mu_2\dot{\theta} + \left(\omega_\theta{}^2 - C_4\cos\nu t^*\right)\theta - \frac{1}{6}\omega_\theta{}^2\theta^3 = -C_3\left(y^*\ddot{y^*} - \dot{y^*}^2\right). \tag{9}$$

In (8) and (9), the dot indicates the derivative with respect to the dimensionless time t^*, and μ_1 and μ_2 respectively denote the damping coefficients of the main system and absorber. In addition, α_3 is the coefficient of the Taylor expansion of the magnetic force with respect to y^{*3}. The term $C_1\ddot{\theta}y^*$ in (8) and terms of the right-hand side in (9) are the quadratic nonlinear coupling effects attributable to the link connection between the main system and the pendulum. Through these terms, the pendulum is moved with twice the frequency of the motion of the main system. Hereinafter in this discussion, the asterisk $(*)$ is omitted for simplification. The dimensionless parameters in (8) and (9) are as follows.

$$\begin{aligned}
C_1 &= \frac{ml}{ML}, \quad C_2 = \frac{(m_0+m)Y_{st}^2}{ML^2},\\
C_3 &= \frac{Y_{st}^2}{Ll}, \quad C_4 = \frac{\nu^2 Y_{st}a_e^*}{l},\\
\alpha_2 &= \frac{(K_{R2}-K_{L2})Y_{st}}{K_{R1}+K_{L1}},\\
\alpha_3 &= \frac{(K_{R3}+K_{L3})Y_{st}^2}{(K_{R1}+K_{L1})},\\
k_{R1} &= \frac{K_{R1}}{K_{R1}+K_{L1}},\\
k_{R2} &= \frac{K_{R2}Y_{st}}{(K_{R1}+K_{L1})},\\
k_{R3} &= \frac{K_{R3}Y_{st}^2}{(K_{R1}+K_{L1})},\\
t^* &= \frac{t}{T}, \quad y^* = \frac{y}{Y_{st}}, \quad \nu = NT, \quad a_e^* = \frac{a_e}{Y_{st}}.
\end{aligned} \tag{10}$$

The values of the dimensionless parameters used in the subsequent theoretical analyses correspond to those in the subsequent experiment. $\mu_1 = 0.0155$, $\mu_2 = 0.01$, $\omega_\theta = 2$, $C_1 = 0.077$, $C_2 = 0.136$, $C_3 = 0.59$, $C_4 = 1.319\nu^2$, $\alpha_2 = 0$, $\alpha_3 = 0.894$, $k_{R1} = 0.5$, $k_{R2} = 0.547$, $k_{R3} = 0.447$, $a_e = 0.0395$.

3 Theoretical analysis using the method of multiple scales

We analyze the dynamics of the main system for the case in which the magnetic force to magnet B changes with the frequency in the neighborhood of the natural frequency of the main system ($\nu \approx 1$); in this case, we sinusoidally move magnet A with the frequency in the neighborhood of the natural linear frequency of the main system. When the natural frequency of the pendulum is tuned to be approximately twice that of the main system, i.e., $\omega_\theta \approx 2$, then the terms $-C_3(y\ddot{y} + \dot{y}^2)$ of the right-hand side of (9) produce a resonance in the pendulum because the frequency of this term, $2\nu(\approx 2)$, is almost equal to the natural frequency of the pendulum $\omega_\theta(\approx 2)$. Through this nonlinear coupling, the energy of the main system is transferred into the absorber and the suppression of the response amplitude of the primary resonance of the main system is carried out. This resonance is based on internal resonance which utilize quadratic nonlinear coupling, that is similar to the autoparametric vibration absorber. However, both absorbers are different in setting the natural frequency of the absorber. The natural frequency of the proposed nonlinear vibration absorber is tuned to be twice the natural frequency of the main system, whereas the natural frequency of the autoparametric vibration absorber is tuned to be one-half the natural frequency of the main system. Furthermore, the another feature of the proposed vibration absorber is that the absorber has no trivial steady state solution in contrast to the conventional autoparametric vibration absorber, i.e., the pendulum cannot be trapped by Coulomb friction existing at the supporting point.

In (8) and (9), the damping force is assumed to be small. Using the order parameter $0 < \epsilon \ll 1$, we put $\mu_1 = \epsilon^{\frac{2}{3}}\hat{\mu}_1$ and $\mu_2 = \epsilon^{\frac{2}{3}}\hat{\mu}_2$, where $\hat{\mu}_1 = O(1)$ and $\hat{\mu}_2 = O(1)$. The excitation amplitude of magnet A is assumed to be small compared with the gap between magnets A and B in the initial static equilibrium state. We set the magnitude of the excitation amplitude quantitatively as $a_e = \epsilon\hat{a}_e$ ($\hat{a}_e = O(1)$). We define a detuning parameter $\sigma = \epsilon^{\frac{2}{3}}\hat{\sigma}$, where $\hat{\sigma} = O(1)$ such as $\nu = 1 + \epsilon^{\frac{2}{3}}\hat{\sigma}$ to express the nearness of the primary resonance and another detuning parameter $\rho = \epsilon^{\frac{2}{3}}\hat{\rho}$ ($\hat{\rho} = O(1)$) such as $\omega_\theta = 2 + \epsilon^{\frac{2}{3}}\hat{\rho}$ to express the tuning of the natural frequency of the pendulum to the neighborhood of twice the natural frequency of the main system. Furthermore, coefficients C_1 and C_3 are assumed to be small as $C_1 = \epsilon^{\frac{1}{3}}\hat{C}_1(\hat{C}_1 = O(1))$ and $C_3 = \epsilon^{\frac{1}{3}}\hat{C}_3(\hat{C}_3 = O(1))$, where C_1 denotes the mass ratio between the main system and absorber, and C_3

denotes the ratio between static displacement of the main system and length of the link in (10). By introducing the multiple time scales of $t_0 = t$ and $t_1 = \epsilon^{\frac{2}{3}} t$, and expanding y and θ as

$$y = \epsilon^{\frac{1}{3}} y_1 + \epsilon y_2 + \cdots, \tag{11}$$

$$\theta = \epsilon^{\frac{1}{3}} \theta_1 + \epsilon \theta_2 + \cdots, \tag{12}$$

we obtain the following equations to order $O(\epsilon^{\frac{1}{3}})$ and to order $O(\epsilon)$:

$$O\left(\epsilon^{\frac{1}{3}}\right): \quad {D_0}^2 y_1 + y_1 = 0, \tag{13}$$

$$\begin{aligned} O(\epsilon): \quad {D_0}^2 y_2 + y_2 = &-2D_0 D_1 y_1 - 2\hat{\mu}_1 D_0 y_1 \\ &+ C_1 \left({D_0}^2 \theta_1\right) y_1 \\ &- \alpha_3 {y_1}^3 + k_{R1} \hat{a}_e \cos \nu t, \end{aligned} \tag{14}$$

$$O\left(\epsilon^{\frac{1}{3}}\right): \quad {D_0}^2 \theta_1 + {\omega_\theta}^2 \theta_1 = 0, \tag{15}$$

$$\begin{aligned} O(\epsilon): \quad & {D_0}^2 \theta_2 + {\omega_\theta}^2 \theta_2 \\ &= -2D_0 D_1 \theta_1 - 2\hat{\mu}_2 D_0 \theta_1 - C_3 y_1 \left({D_0}^2 y_1\right) \\ &\quad - C_3 (D_0 y_1)^2 + \frac{1}{6} {\omega_\theta}^2 {\theta_1}^3, \end{aligned} \tag{16}$$

where $D_n = \partial / \partial t_n$. The solutions of (13) and (15) are written in the form of

$$\begin{aligned} y_1 = &A_1(T_1, T_2) \exp(i T_0) \\ &+ \bar{A}_1(T_1, T_2) \exp(-i T_0), \end{aligned} \tag{17}$$

$$\begin{aligned} \theta_1 = &A_2(T_1, T_2) \exp(i \omega_\theta T_0) \\ &+ \bar{A}_2(T_1, T_2) \exp(-i \omega_\theta T_0). \end{aligned} \tag{18}$$

Substituting (17) and (18) into (14) and (16) and using polar notation $A_1 = \frac{1}{2} a_1 \exp(i \psi_1)$ and $A_2 = \frac{1}{2} a_2 \exp(i \psi_2)$, we obtain the following solvability conditions of (14) and (16).

$$\begin{aligned} \frac{da_1}{dt} = &-\mu_1 a_1 + \frac{1}{4} C_1 {\omega_\theta}^2 a_1 a_2 \sin \gamma_2 \\ &+ \frac{1}{2} k_{R1} \hat{a}_e \sin \gamma_1, \end{aligned} \tag{19}$$

$$\frac{da_2}{dt} = -\mu_2 a_2 - \frac{1}{2\omega_\theta} C_3 {a_1}^2 \sin \gamma_2, \tag{20}$$

$$\begin{aligned} a_1 \frac{d\psi_1}{dt} = &-\frac{1}{4} C_1 \omega_\theta^2 a_1 a_2 \cos r_2 + \frac{3}{8} \alpha_3 {a_1}^3 \\ &- \frac{1}{2} k_{R1} \hat{a}_e \cos \gamma_1, \end{aligned} \tag{21}$$

$$a_2 \frac{d\psi_2}{dt} = -\frac{1}{2\omega_\theta} C_3 {a_1}^2 \cos \gamma_2, \tag{22}$$

$$\gamma_1 = \sigma T_1 - \psi_1, \qquad \gamma_2 = \psi_2 - 2\psi_1 + \rho T_1. \tag{23}$$

The first-order approximate solutions of (8) and (9) are

$$y = a_1 \cos(\nu t - \gamma_1) \quad + O(\epsilon), \tag{24}$$

$$\theta = a_2 \cos(2\nu t + \gamma_2 - 2\gamma_1) \quad + O(\epsilon). \tag{25}$$

Eliminating ψ_1 and ψ_2 from (21) through (23), (21) and (22) can be written as follows:

$$\begin{aligned} a_1 \frac{d\gamma_1}{dt} = &\sigma a_1 + \frac{1}{4} C_1 \omega_\theta^2 a_1 a_2 \cos r_2 - \frac{3}{8} \alpha_3 {a_1}^3 \\ &+ \frac{1}{2} k_{R1} \hat{a}_e \cos \gamma_1, \end{aligned} \tag{26}$$

$$\begin{aligned} a_2 \frac{d\gamma_2}{dt} = &\rho a_2 - \frac{3}{4} \alpha_3 {a_1}^2 a_2 + \frac{C_1 \omega_\theta^2}{2} {a_2}^2 \cos \gamma_2 \\ &+ k_{R1} \hat{a}_e \frac{a_2}{a_1} \cos \gamma_1 - \frac{1}{2\omega_\theta} C_3 {a_1}^2 \cos \gamma_2. \end{aligned} \tag{27}$$

These solvability conditions govern the dynamics of the amplitude a_1 and the phase γ_1 of the main system, and the amplitude a_2 and the phase γ_2 of the pendulum. For the steady-state solution, letting $da_1/dt = da_2/dt = d\gamma_1/dt = d\gamma_2/dt = 0$, and (19), (20), (26), and (27) are combined into algebraic equations whose solutions are steady-state amplitudes a_1 and a_2:

$$c_6 {a_1}^6 + c_4 {a_1}^4 + c_2 {a_1}^2 - c_0 = 0, \qquad a_2 = \frac{C_3 {a_1}^2}{4\phi}, \tag{28}$$

where the coefficients of each term are expressed by system parameters as

$$\begin{aligned} c_6 = &4{C_1}^2 {C_3}^4 {\mu_2}^2 + 4{C_1}^2 {C_3}^4 (2\sigma - \rho)^2 \\ &+ 9{C_3}^2 {\alpha_3}^2 \phi^4 + 12 C_1 {C_3}^3 (2\sigma - \rho) \alpha_3 \phi^2, \\ c_4 = &32 \mu_1 \mu_2 C_1 {C_3}^3 \phi^2 - 32\sigma (2\sigma - \rho) C_1 {C_3}^3 \phi^2 \\ &- 48\sigma {C_3}^2 \alpha_3 \phi^4, \\ c_2 = &64 {\mu_1}^2 {C_3}^2 \phi^4 + 64 \sigma^2 {C_3}^2 \phi^4, \\ c_0 = &16 {C_3}^2 \phi^4 {k_{R1}}^2 \hat{a}_e^2, \quad \phi = \sqrt{{\mu_2}^2 + (2\sigma - \rho)^2}. \end{aligned} \tag{29}$$

4 Effect of vibration absorber

4.1 Suppression of response in the main system under small excitation amplitude

Frequency response curve of the main system in the case where the absorber is fixed is shown in Fig. 4, where the solid and broken lines, respectively, denote stable and unstable steady state amplitudes. Because of the nonlinearity of the restoring force, the frequency response curve is bent and the resonance peak is different from the linear natural frequency ($\sigma = 0$); it is at $\sigma = 0.13$ ($\nu = 1.13$). The hysteresis exists in the frequency response curve. The frequency response curves of the main system and the absorber in the case where the absorber is in action under small excitation amplitude are shown respectively in Figs. 5(a) and 5(b); for reference, the frequency response curve in the case where the absorber is fixed is superimposed as a dashed line in Fig. 5(a). The absorber suppresses the resonant amplitude, and the hysteresis is not visible. As shown in the study of the two-beam two-mass metallic structure [12], overhang [1] produced in the case of the autoparametric vibration absorber is not produced in this proposed absorber.

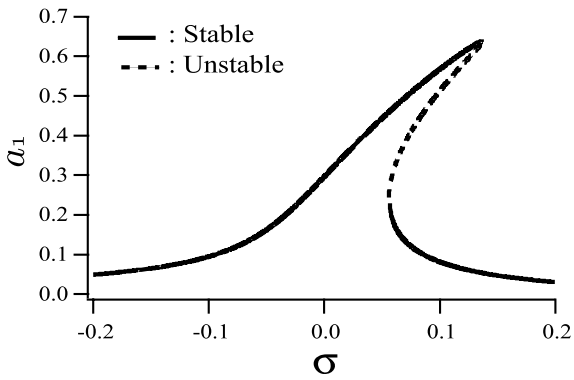

Fig. 4 Frequency response curve of the main system in the case where the absorber is fixed

4.2 Response under large excitation amplitude

The frequency response curves for the main system in case with absorber under large excitation amplitude are shown in Fig. 6; solid lines and broken lines, respectively, represent stable and unstable steady state solutions. Figure 6(a) depicts the case for an absorber with small damping coefficient, $\mu_2 = 0.01$, and Fig. 6(b) presents the case for an absorber with large damping coefficient, $\mu_2 = 0.5$. Comparison with the case under small excitation amplitude shows that the lower and higher peaks are produced, and unstable steady state solutions exist in the neighborhood of $\nu = 1$. By increasing the damping of the absorber, we can eliminate the lower peak and reduce the higher peak and thereby render unstable steady state solutions stable, as shown in Fig. 6(b). However, the effect of the absorber by increasing damping limits resonance amplitude reduction. In other words, when the damping of the absorber becomes greater than some threshold value, the response amplitude of the main system is not reduced beyond some threshold amplitude in spite of increased damping of the absorber. The reason is the cubic nonlinearity of the restoring force acting on

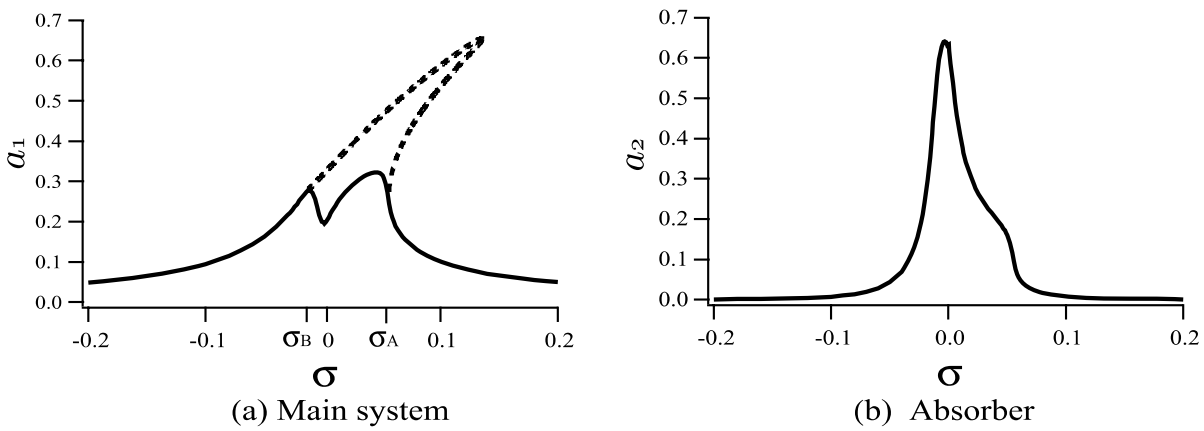

Fig. 5 Frequency response curves in the case where the absorber is in action under small excitation amplitude ($a_e = 0.0395$)

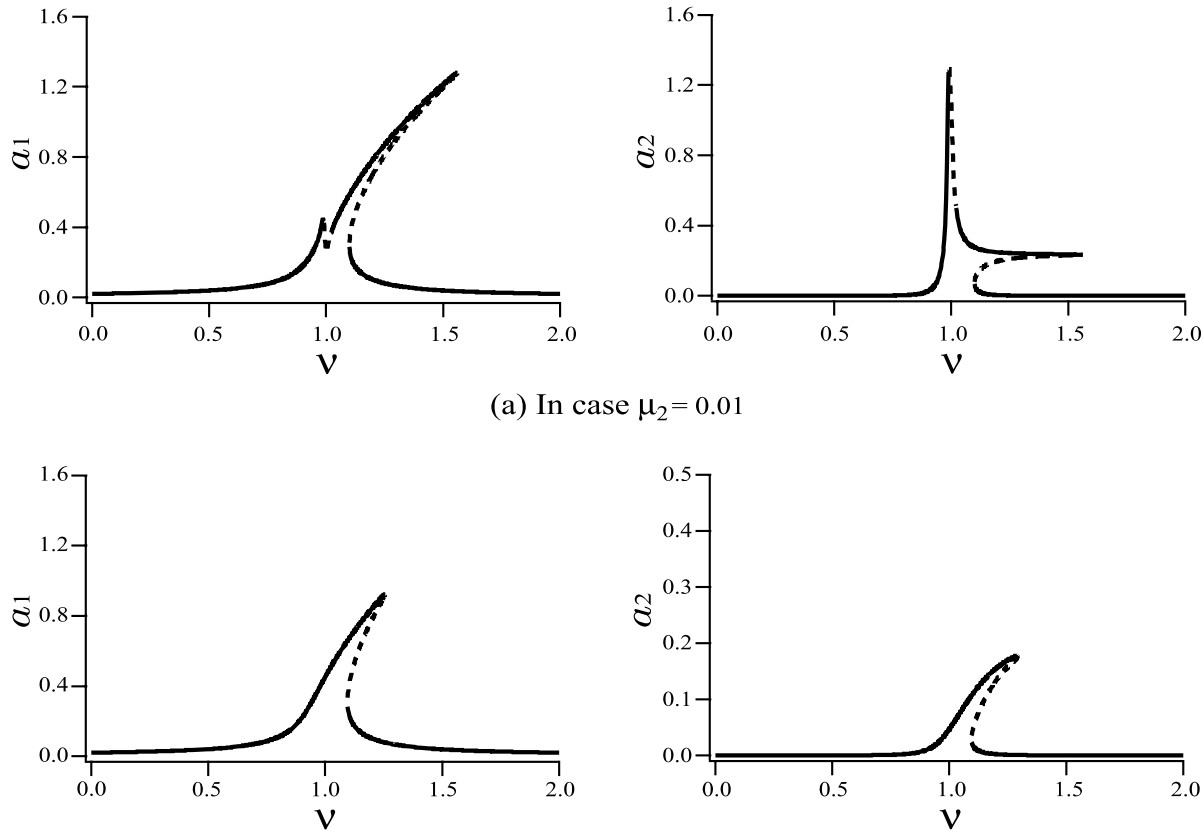

Fig. 6 Frequency response curve of the main system with absorber of various damping coefficients ($a_e = 0.08$)

the main system. Generally, the nonlinear vibration absorber acts only in the case when the excitation frequency is in the neighborhood of the linear natural frequency of the main system (in the case of primary resonance, the response amplitude can be reduced only if the excitation frequency is near the linear natural frequency) because the reduction method is based on mode coupling. Under large excitation amplitude, the frequency response curve is bent severely and the peak is located far away from the linear natural frequency; for the main system subjected to the linear restoring force, the increase of damping very effectively reduces the peak of the frequency response curve (see the Appendix for the linear system). For that reason, it is impossible to reduce sufficiently the peak of the response amplitude of the main system subjected to the cubic nonlinear restoring force.

5 Experimental results

The experimental apparatus is shown in Figs. 7 and 8. The main system M, which is subjected to repulsive magnetic forces from both sides, can move freely in the y-direction on a slide bearing that is mounted on the horizontal plane. We move magnet A in the y-direction as $y_0 = a_e \cos Nt$ by an electromagnetic shaker (Type 513-B; EMIC Corp.). As shown in Fig. 8, the dimension of magnets A and A' are $50 \times 50 \times 18$ mm; the dimension of magnets on both sides of the main system are $40 \times 20 \times 10$ mm. The dimensions and mass for the main system and the absorber are as follows: $y_{st} = 43$ mm, $M = 0.562$ kg, $m_0 = 0.25$ kg, $m = 0.13$ kg, $a_e = 1.7$ mm, $L = 96$ mm, $l = 32$ mm, $l_0 = 100$ mm, $\omega_y/2\pi T = 1.38$ Hz, and $\omega_\theta/2\pi T = 2.76$ Hz.

The motions of magnet A and the main system are measured using laser displacement sensors (LB-01;

Fig. 7 Experimental setup

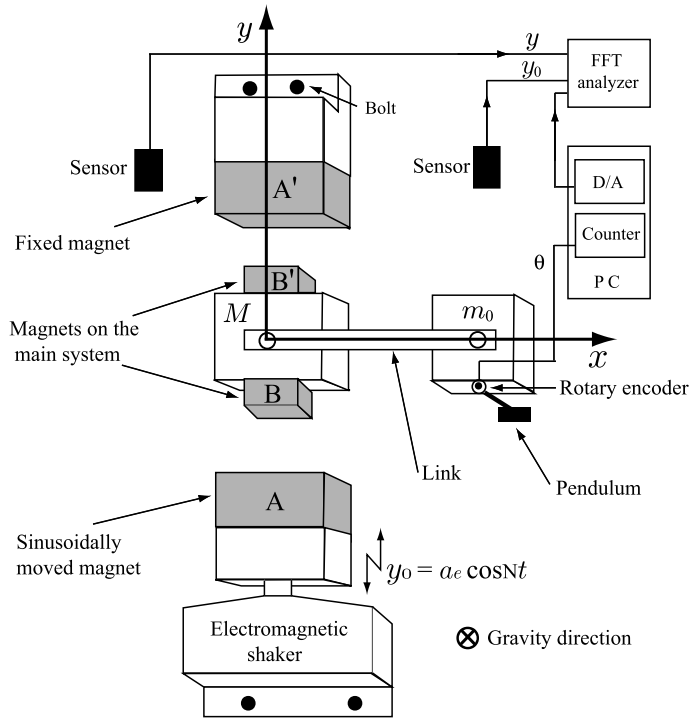

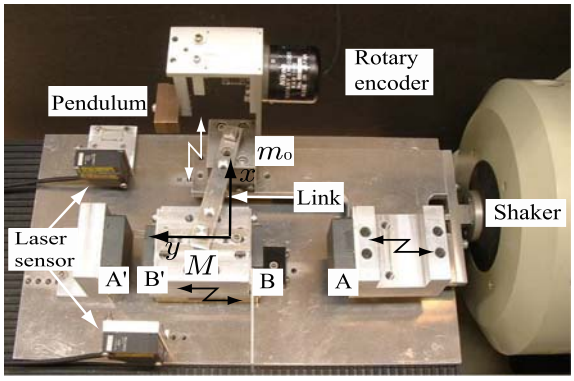

Fig. 8 Image of the experimental apparatus

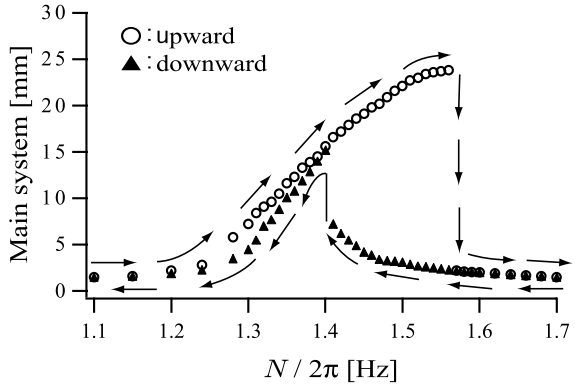

Fig. 9 Experimental frequency response curve of the main system for the case in which the absorber is fixed ($a_e = 1.7$ mm)

Keyence Co.). A mass m_0 is connected to the main system by a link; it can move freely in the x-direction. A pendulum with tip mass m is supported by a radial bearing. The angle is measured using a rotary encoder (RXB1000; Nikon Corp.). The connection between the absorber and the main system by the link excites the pendulum-type absorber with twice the frequency of the motion of the main system. Then under the tuning condition by which the natural frequency of the pendulum is approximately twice the natural frequency of the main system, the resonance occurs both in the absorber and main system.

Figure 9 presents the experimentally obtained frequency response curve of the main system for the case in which the absorber is fixed. Hysteresis exists in the frequency response curve. The circles denote upward sweeping from low frequency to high frequency; triangles denote downward sweeping from high frequency to low frequency. The arrows indicate the sweep of the excitation frequency. The jump phenomena occur in

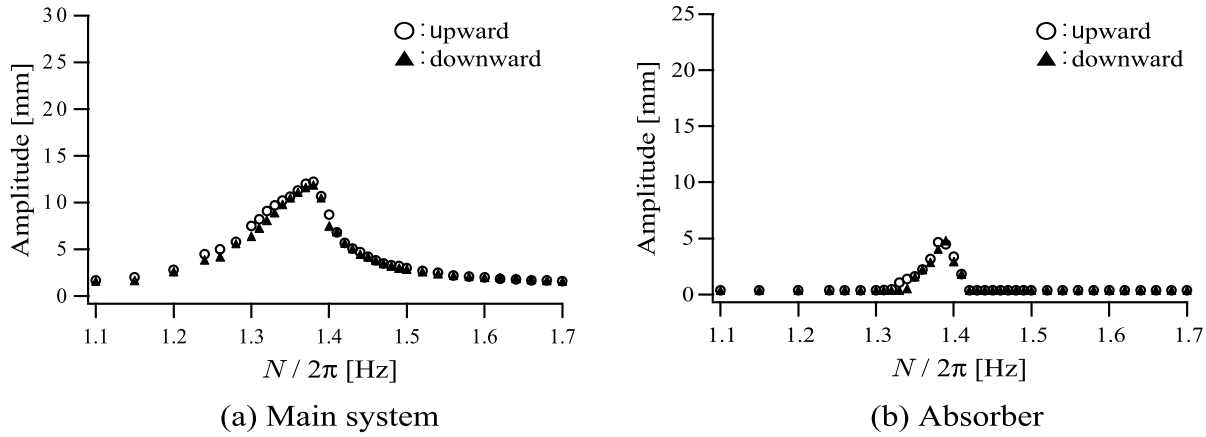

Fig. 10 Experimental frequency response curves of the main system for the case in which the absorber is in action ($a_e = 1.7$ mm)

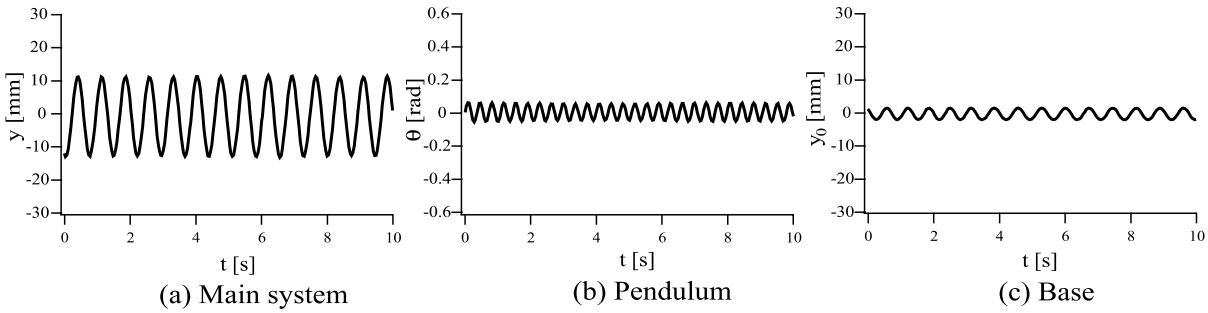

Fig. 11 Time history in primary resonance in the case where the absorber is in action

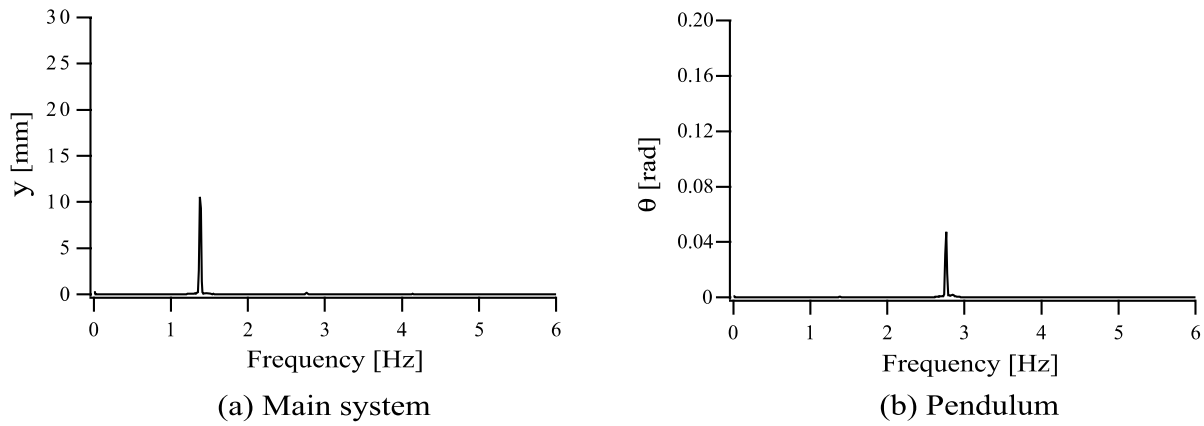

Fig. 12 Comparison of main system and absorber response frequencies

the frequency sweep. In the case of upward sweeping, the resonant peak occurs at $N/2\pi = 1.56$ Hz and the amplitude is 24 mm. Figure 10 depicts the experimental frequency response curve of the main system and absorber in the case where the absorber is in action under small excitation amplitude. In contrast to

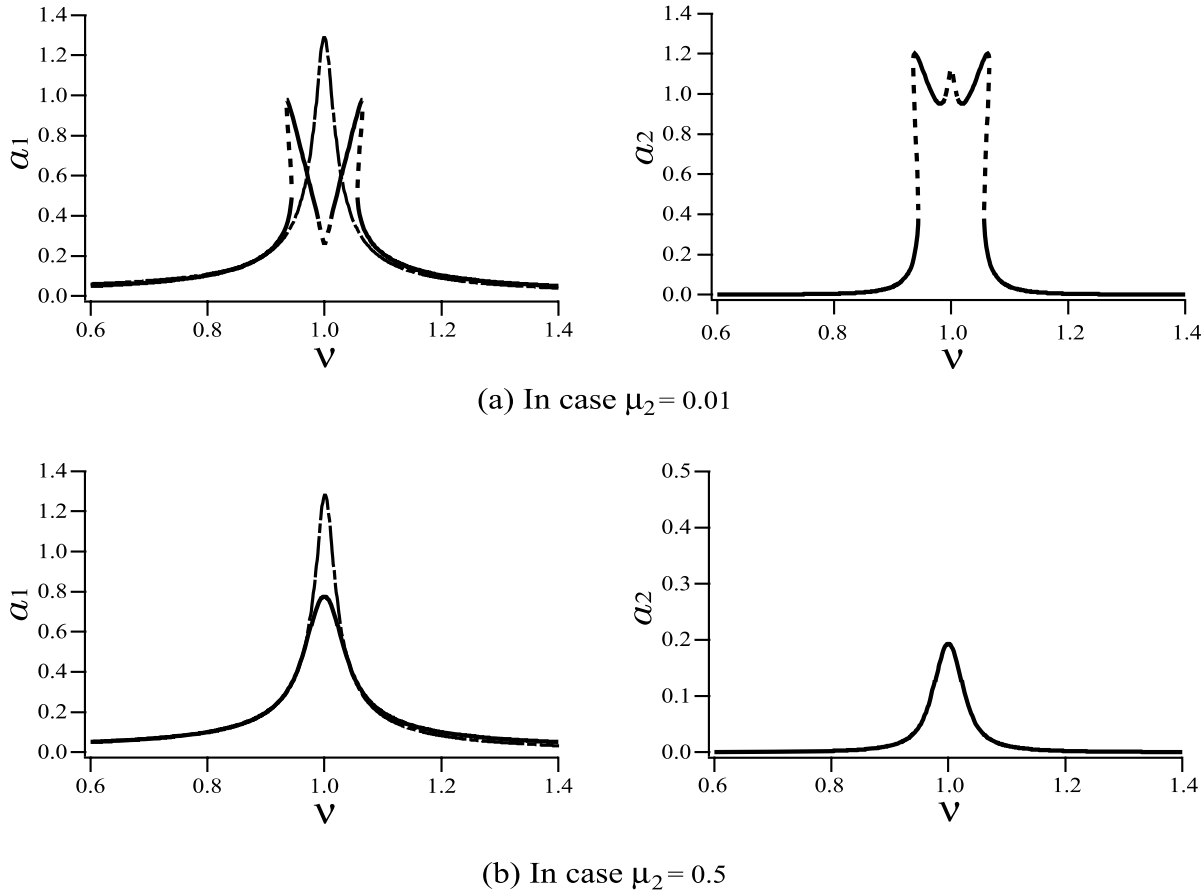

Fig. 13 Frequency response curve of the main system with absorber of various damping ($a_e = 0.08$, --- : In case when the absorber is fixed)

the case in which the absorber is fixed, no hysteresis exists in the frequency response curve; also, no jump phenomenon appears in the frequency sweep. The resonant peak occurs at $N/2\pi = 1.38$ Hz. It is apparent from comparison between Figs. 9 and 10 that the nonlinear vibration absorber reduces the response amplitude; the maximum amplitude is 12.5 mm and the reduction ratio is about 45%. Compared to the analytical results presented in Fig. 5, despite a small quantitative discrepancy, qualitative agreement is apparent; the resonant amplitude is reduced and hysteresis disappears in the frequency response curve in case under small excitation amplitude. Figures 11(a), (b), and (c), respectively, depict the time histories of the main system, the absorber, and the excitation of magnet A for the case with absorber. The excitation frequency is 1.38 Hz, which gives the peak of the frequency response curve in case with the absorber, as shown in Fig. 10. The FFT analysis shown in Fig. 12 also shows that the pendulum oscillates with twice the frequency of the motion of the main system.

6 Conclusions

In this paper, we investigated a new type of nonlinear vibration absorber whose natural frequency was tuned to be twice the natural frequency of the main system, whereas the natural frequency of the autoparametric vibration absorber is tuned to be one-half the natural frequency of the main system. Then the absorber is required to oscillate at twice the frequency of the motion of the main system. For that purpose, we proposed a configuration of the absorber that is connected to the main system by a link. In addition, the proposed absorber presents an important advantage: the absorber

cannot be trapped by unexpected circumstance (e.g., large Coulomb friction), because the absorber has no trivial steady state solution, in contrast to the conventional autoparametric vibration absorber.

We theoretically analyze the effectiveness of the proposed absorber on the main system subjected to cubic nonlinear restoring force under primary resonance. The characteristics of the absorber are as follows:

1. In the case of small excitation amplitude, an overhang of the frequency response curve is not produced, in contrast to the autoparametric vibration absorber; there is no frequency range for which the absorber makes the response amplitude larger than that in the case without the absorber.
2. In the case of large excitation amplitude, unstable steady state solutions exist in the neighborhood of the natural frequency of the main system, the increase of the damping of the absorber can stabilize unstable steady state solutions.
3. A limitation pertains to the resonance amplitude reduction for the case in which the frequency response curve is bent severely and the peak of the frequency response curve differs greatly from the linear natural frequency because the nonlinear absorber is based on mode coupling.

For the case of small excitation amplitude, we compared the experimentally obtained frequency response curves between the cases in which the absorber is fixed and in action. The effectiveness of the absorber is confirmed experimentally under small excitation amplitude.

Appendix: Response in main system subjected to linear restoring force under the present nonlinear vibration absorber

By setting the parameters α_2 and α_3 to zero, the theoretical results in Sect. 4 correspond to those in the case where the restoring force acting the main system is linear.

The frequency response curves of the main system and the absorber under large excitation amplitude shown in Fig. 13; (a) and (b) correspond respectively to the cases of small and large damping of the absorber, $\mu_2 = 0.01$ and $\mu_2 = 0.5$. The solid and broken lines respectively represent stable and unstable steady state solutions. The dashed and dotted line shows the frequency response curve for the case in which the absorber is fixed. In contrast to Fig. 6, an increase of the excitation amplitude produces an overhang. By increasing the damping of the absorber, the overhang disappears and the peak of the frequency response curve is sufficiently reduced because the excitation frequency at the peak of the frequency response curve is equal to the natural frequency of the main system.

References

1. Haxton, R.S., Barr, A.D.S.: The autoparametric vibration absorber. Trans. ASME J. Eng. Ind. **94**, 119–125 (1972)
2. Tondl, A., Ruijgrok, T., Verhulst, F., Nabergoi, R.: Autoparametric Resonance in Mechanical Systems. Cambridge University Press, Cambridge (2000)
3. Vyas, A., Bajaj, A.K.: Dynamics of autoparametric vibration absorber using multiple pendulums. J. Sound Vib. **246**(1), 115–135 (2001)
4. Vyas, A., Bajaj, A.K., Raman, A.: Dynamics of structures with wideband autoparametric vibration absorbers: theory. In: Proceedings of the Royal Society of London Series A. Mathematical Physical and Engineering Sciences, vol. 460, pp. 1857–1880 (2004)
5. Vyas, A., Bajaj, A.K., Raman, A.: Dynamics of structures with wideband autoparametric vibration absorbers: experiment. In: Proceedings of the Royal Society of London Series A. Mathematical Physical and Engineering Sciences, vol. 460, pp. 1547–1581 (2004)
6. Mustafa, G., Ertas, A.: Dynamics and bifurcation of a coupled column-pendulum oscillator. J. Sound Vib. **182**(3), 393–413 (1995)
7. Cuvalci, O., Ertas, A.: Pendulum as vibration absorber for flexible structures: experiments and theory. ASME J. Vib. Acoust. **118**, 558–566 (1996)
8. Mook, D.T., Plaut, R.H., Haquang, H.: The influence of an internal resonance on non-linear structure vibrations under subharmonic resonance conditions. J. Sound Vib. **102**(4), 473–492 (1985)
9. Yabuno, H., Endo, Y., Aoshima, N.: Stabilization of 1/3-order subharmonic resonance using an autoparametric vibration absorber. ASME J. Vib. Acoust. **121**, 309–315 (1999)
10. Nayfeh, A.H., Mook, D.T.: Nonlinear Oscillations. Wiley, New York (1979)
11. Nayfeh, A.H.: Nonlinear Interactions: Analytical, Computational, and Experimental Methods. Wiley, New York (2000)
12. Haddow, A.G., Barr, A.D.S., Mook, D.T.: Theoretical and experimental study of modal interaction in a two-degree-of-freedom structure. J. Sound Vib. **97**(3), 451–473 (1984)
13. Yabuno, H., Seino, T., Yoshizawa, M., Tsujioka, Y.: Dynamical behavior of a levitated body with magnetic guides. JSME Int. J. Ser. 3 **32**(3), 428–435 (1989)
14. Yabuno, H., Fujimoto, N., Yoshizawa, M., Tsujioka, T.: Bouncing and pitching oscillations of a magnetically levitated body due to the guideway roughness. JSME Int. J. Ser. 3 **34**(2), 192–199 (1991)